

Oxygen isotope effect on quasiparticle and optical properties in cupratesE. Schachinger^{1,*} and J. P. Carbotte^{2,3}¹*Institute of Theoretical and Computational Physics, Graz University of Technology, A-8010 Graz, Austria*²*Department of Physics and Astronomy, McMaster University, Hamilton, Ontario, Canada N1G 2W1*³*The Canadian Institute for Advanced Research, Toronto, Ontario, Canada M5G 1Z8*

(Received 8 October 2009; revised manuscript received 15 December 2009; published 21 January 2010)

In a recent nodal direction angular-resolved photoemission spectroscopy (ARPES) study of the renormalized electronic dispersion curves in $\text{Bi}_2\text{Sr}_2\text{CaCu}_2\text{O}_{8+\delta}$, small changes in the “kink” structure around 70 meV were observed on ^{16}O to ^{18}O substitution. Based on the Eliashberg equations generalized to include the d -wave symmetry of the superconducting gap, we show that these results are incompatible with predominant coupling to a single oxygen-phonon mode. They can be understood in a model where a peak centered at ~ 60 meV comprising of only 10% of the total area under the electron-boson interaction spectral density obtained by a maximum entropy inversion of nodal direction of ARPES data, is assigned to phonons and shifted in energy by the 6% expected for oxygen isotope effect. The remaining background with 90% of the area comes from spin fluctuations. Based on a momentum-averaged electron-boson spectral density recovered from optical scattering-rate data, we study corresponding isotope shifts expected in the optical response.

DOI: [10.1103/PhysRevB.81.014519](https://doi.org/10.1103/PhysRevB.81.014519)

PACS number(s): 74.20.Mn, 74.25.Kc, 74.72.-h

I. INTRODUCTION

There is a large body of evidence in the high T_c cuprates that the charge carriers are coupled to a bosonic spectrum although the exact nature of the bosons involved remains controversial.^{1–18} In angular-resolved photoemission spectroscopy (ARPES) the boson coupling manifests itself as “kinks” in the renormalized electronic-dispersion curves which originate from structure in the quasiparticle self-energy as a function of energy.^{1–10,17} ARPES is a directional probe giving information on the momentum dependence of quasiparticle properties along any direction in the Brillouin zone. However, it is surface sensitive. A complimentary method is the optical conductivity as a function of energy.^{11–16,18–20} This is a bulk probe, applicable to a large range of materials but it provides only momentum-averaged information. Nevertheless, valuable information on boson structure has been extracted from considerations of the optical self-energy^{12–15} obtained from the generalized Drude formula for the optical conductivity. Coupling to a particular Einstein mode manifests itself as a sharp rise in the optical scattering rate. Additional information can be obtained from the analysis of tunneling characteristics.^{21,22} This includes recent scanning-tunneling microscope (STM) studies^{23–25} which were aimed more directly at boson structures. The techniques just described do not on their own allow a definite identification of the nature of the excitation involved, i.e., phonons, spin fluctuations, or some other boson. Nevertheless, the scale and range in energy as well as the shape of the distribution of modes involved in the scattering can help in this regard. The change in boson structure seen with change in direction of momentum as in ARPES, for example, can also provide important information, so can changes with increasing temperature or isotope substitution.

There have been many studies of the effect of oxygen isotope substitutions $^{16}\text{O} \rightarrow ^{18}\text{O}$ on boson structure which go beyond the simple observation of a shift in the critical temperature,²⁶ small for optimum doping but larger in the

underdoped regime^{26–28} due to energy dependence in the density of states and/or pseudogap formation. ARPES studies include the work of Lanzara *et al.*²⁹ and, later, Gweon *et al.*³⁰ who found large shifts even at high energies. On the other hand, an optical study by Wang *et al.*³¹ found no evidence of an isotope shift. Recent STM work²⁵ has shown a shift in a 52 meV structure of about the expected amount for an oxygen mode but this may be explained in terms of inelastic tunneling through the barrier.^{32–34} New high-precision low-energy ARPES data³⁵ on a high-quality single crystal of optimally doped $\text{Bi}_2\text{Sr}_2\text{CaCu}_2\text{O}_{8+\delta}$ ($\text{Bi}2212$) with a T_c of 92 K have revealed a 3.4 meV shift of the kink at 69 meV seen in the nodal direction for $^{16}\text{O} \rightarrow ^{18}\text{O}$ substitution with modifications confined mainly to the kink region.

The analysis presented here is based on Eliashberg theory first considered for an electron-phonon system^{36–39} but also widely used in the nearly antiferromagnetic Fermi-liquid model (NAFLM) based on spin fluctuations⁴⁰ as reviewed by Chubukov *et al.*⁴¹ In support of the NAFLM approach, recent numerical solutions of the Mott-Hubbard model suggest that in the high- T_c cuprates retarded interactions do provide most of the pairing^{42,43} with the energy scale set by the size of the antiferromagnetic exchange constant J . These calculations do not support the suggestion by Anderson⁴⁴ that the energy scale for the retardation might be much higher and set by the Hubbard U which would imply nonretarded pairing. Another mechanism considered in the literature is kinetic-energy-driven pairing for which it is the kinetic rather than the potential energy which is reduced as the temperature is lowered below T_c . This mechanism can also be treated in an Eliashberg formalism through a phenomenological reduction in quasiparticle scattering brought about by the freezing out of low energy excitations.^{45–47}

In the formulation of the Eliashberg theory applied here, the interaction between the charge carriers and the exchange bosons is described by a spectral function $I^2F(\omega)$ which is to be the sum of a spin-fluctuation contribution $I^2\chi(\omega)$ and a phonon part $\alpha^2F(\omega)$. Assuming d -wave symmetry for the

superconducting gap, this spectral function acquires an additional dependence on angle θ , the polar angle in the CuO₂ Brillouin zone, with $\theta=0$ indicating the nodal direction. If we consider, for instance, coupling to a resonant mode at (π, π) , Fermi-surface to Fermi-surface transitions caused by scattering off such a mode might not be possible in the nodal direction because of the particular geometry of the Fermi surface involved. But they could become possible as the antinodal direction is approached and, thus, it appears that the $I^2F(\omega)$ spectrum for the antinodal direction will be much different from its nodal direction value. This can be probed with ARPES. In contrast, for optics data a θ -averaged spectrum $I^2F(\omega)$ is required.

We provide here a more detailed analysis of the nodal direction ARPES data upon $^{16}\text{O} \rightarrow ^{18}\text{O}$ substitution than was given in Ref. 35 and in our own brief report.²⁰ We want to understand better what these results tell us about the role phonons might play in the mechanism of superconductivity in the high T_c cuprates. We begin with a model calculation which is aimed at understanding how quasiparticle properties would shift if the primary coupling were due to an oxygen phonon. Section II A deals with the normal state and Sec. II B with the superconducting state assuming a d -wave gap. In Sec. III we consider the optical self-energy which is different but analogous to the quasiparticle self-energy of ARPES. In Sec. IV we deal more specifically with the case of Bi2212. We base our discussion on a realistic form for the electron-boson spectral density previously obtained by Schachinger and Carbotte¹¹ from a maximum entropy inversion of the high-precision nodal direction ARPES data reported by Zhang *et al.*¹⁷ This spectrum consists of a broad peak centered at 65 meV superimposed on a large background extending to 400 meV. Shifting the peak by 6% in energy and leaving the major part of the spectrum unaltered produces changes in the quasiparticle renormalization that are large enough to explain the data of Iwasawa *et al.*³⁵ A parallel discussion of optical properties is also given but now based on a momentum-averaged spectral density $I^2F(\omega)$ obtained from a maximum entropy inversion of the optical scattering rate. In Sec. V we give a brief conclusion.

II. MODEL CALCULATIONS

A. Normal state

We begin with a model in which the charge carriers are coupled to a single Einstein mode of energy ω_E . The electron-boson spectral density is $A\delta(\omega - \omega_E)$ with A the area under the Dirac δ -function $\delta(x)$. The resulting quasiparticle self-energy in the normal state at zero temperature ($T=0$) is

$$\Sigma(\omega) = \Sigma_1(\omega) + i\Sigma_2(\omega) = A \ln \left| \frac{\omega_E - \omega}{\omega_E + \omega} \right| - i\pi A \theta(|\omega| - \omega_E) \quad (1)$$

with $\theta(x)$ a step function. Under isotopic substitution $^{16}\text{O} \rightarrow ^{18}\text{O}$, $\omega_E \rightarrow \gamma\omega_E$, and the coupling $A \rightarrow \gamma A$ so that the mass enhancement parameter $\lambda = 2A/\omega_E$ remains unchanged,

and $\gamma = \sqrt{16/18} = 0.94$ corresponding to a 6% reduction in ω_E . We denote the self-energy of the isotope-substituted material by $\Sigma_{\text{iso}}(\omega)$. Its imaginary part jumps from zero to $-\pi\gamma A$ at $\gamma\omega_E$ rather than to $-\pi A$ at ω_E as seen in Eq. (1). The change in frequency of the sharp onset of the scattering gives the change in ω_E while the change in the magnitude of the scattering rate which is constant above ω_E gives the change in the electron-phonon coupling, i.e., of the area under the electron-phonon spectral density $\alpha^2F(\omega)$. Both quantities change by the same percentage for phonons. Modifications to the real part of the self-energy given by

$$\Sigma_{1,\text{iso}}(\omega) = \gamma A \ln \left| \frac{\gamma\omega_E - \omega}{\gamma\omega_E + \omega} \right| \quad (2)$$

are more complex. This quantity remains unchanged in the limit $\omega \ll \omega_E$ where it is linear in ω with slope given by the mass enhancement parameter λ which does not depend on isotope. Its logarithmic singularity, however, is shifted to $\gamma\omega_E$ and at $\omega \gg \omega_E$ it varies as $2\gamma^2 A \omega_E / \omega$. It is clear from this analysis that the changes in $\Sigma(\omega)$ due to $^{16}\text{O} \rightarrow ^{18}\text{O}$ substitutions depend on the value of ω considered.

Similar changes arise when a distributed phonon spectrum is used. In this case the quasiparticle self-energy $\Sigma(T, \omega)$ in the nodal direction is given by^{11,16,48-52}

$$\Sigma(T, \omega) = \int_0^\infty d\Omega I^2F(\Omega) \int_{-\infty}^\infty d\nu \tilde{N}(T, \nu) \left[\frac{n(T, \Omega) + f(T, -\nu)}{\omega - \Omega - \nu + i0^+} + \frac{n(T, \Omega) + f(T, \nu)}{\omega + \Omega - \nu + i0^+} \right], \quad (3)$$

which is valid in the superconducting as well as normal state. Here, $n(T, \Omega)$ and $f(T, \nu)$ are Bose and Fermi distribution, respectively, and $\tilde{N}(T, \nu)$ is the self-consistent electronic density of states (DOS). For the normal state with a constant density of states $N(0)$ around the Fermi energy $\tilde{N}(T, \nu)$ would reduce to one. Equation (3) holds for any system with effective DOS $\tilde{N}(T, \nu)$ and electron-boson spectral function $I^2F(\Omega)$. For a superconductor, $\tilde{N}(T, \nu)$ will involve the superconducting gap and have an inverse square-root singularity for s -wave symmetry of the gap function and a logarithmic singularity for d -wave symmetry in a clean limit system. It is through $\tilde{N}(T, \nu)$ that the superconducting gap enters the nodal direction self-energy.

Starting with normal-state results, they are illustrated in Fig. 1 for the case of a Lorentzian distribution with area $A = 20.7$ meV, $\lambda = 1.2$, its peak at $\omega_L = 36.4$ meV, and of width $\Gamma = 3$ meV in the normal state at 10 K. The (red) curves in the middle frame of Fig. 1, dashed-dotted and dotted, respectively, give $\alpha^2F(\omega)$ and $\alpha^2F_{\text{iso}}(\omega)$ to which the right-hand scale applies. Also shown are thin vertical lines which identify the frequency of the peak in the spectral density at $\omega_L = 36.4$ meV for ^{16}O and $\omega_{L,\text{iso}} = 34.3$ meV for ^{18}O in the other two frames. The top frame of Fig. 1 gives the imaginary part of the self-energy $-\Sigma_2(\omega)$ vs ω in meV. The solid

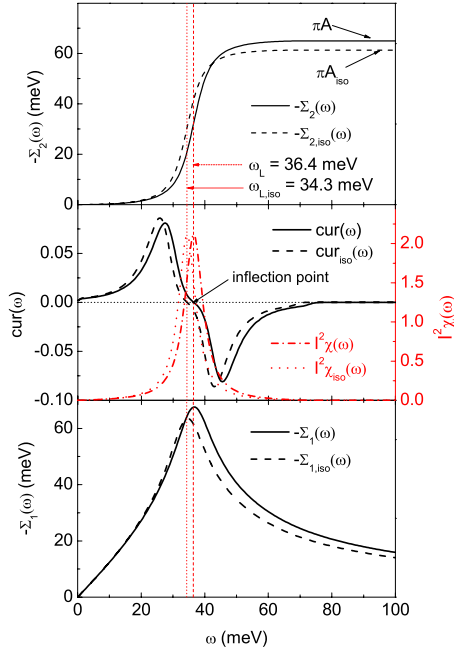


FIG. 1. (Color online) Top frame: minus the imaginary part of the quasiparticle self-energy $-\Sigma_2(\omega)$ (^{16}O solid and ^{18}O dashed lines) vs the energy ω for a Lorentzian model $\alpha^2F(\omega)$ (see middle frame) peaked around 36.4 meV in the normal state at $T=10$ K. Middle frame: the curvature $\text{cur}(\omega)$ of $-\Sigma_2(\omega)$ vs ω (left-hand scale, solid and dashed line). The dashed-dotted line shows the Lorentzian model $\alpha^2F(\omega)$ (right-hand scale) for ^{16}O while the dotted line corresponds to ^{18}O . Bottom frame: the same as the top frame but now for $-\Sigma_1(\omega)$.

(black) line is for $-\Sigma_2(\omega)$ and the dashed (black) line is for $-\Sigma_{2,\text{iso}}(\omega)$. The onset of scattering is no longer sharp and the smearing about ω_L reflects the distribution of modes in $\alpha^2F(\omega)$. Nevertheless, for a Lorentzian spectrum there is an inflection point precisely at ω_L . In the middle frame we show the result for the curvature associated with the quasiparticle scattering rate

$$\text{cur}(\omega) = \frac{\Sigma_2''(\omega)}{[1 + \Sigma_2'(\omega)]^{3/2}} \quad (4)$$

and $\text{cur}(\omega)=0$ at the energy of the inflection point. In Eq. (4), $\Sigma_2'(\omega)$ is the first and $\Sigma_2''(\omega)$ is the second derivative of $\Sigma_2(\omega)$ with respect to ω . Returning to the top frame of Fig. 1 we see that at $\omega \gg \omega_L$ the two curves become parallel and saturate to πA and $\gamma\pi A = \pi A_{\text{iso}}$, respectively. They also cross somewhat above ω_L . All these features must correlate in any definitive identification of an isotope effect. In the bottom frame of Fig. 1 we give our results for the real part of the self-energy, $-\Sigma_1(\omega)$. The (black) solid and dashed curves merge at small ω as expected because they both correspond to the same value of the mass enhancement parameter λ . Note that the logarithmic singularity of the δ -function case has been considerably smeared out even though our Lorentzian spectrum for the distribution of modes is not very broad. The maxima in these curves do not fall exactly at ω_L and $\gamma\omega_L \equiv \omega_{L,\text{iso}}$ but rather at 36.7 and 34.6 meV, respectively. The amplitude of

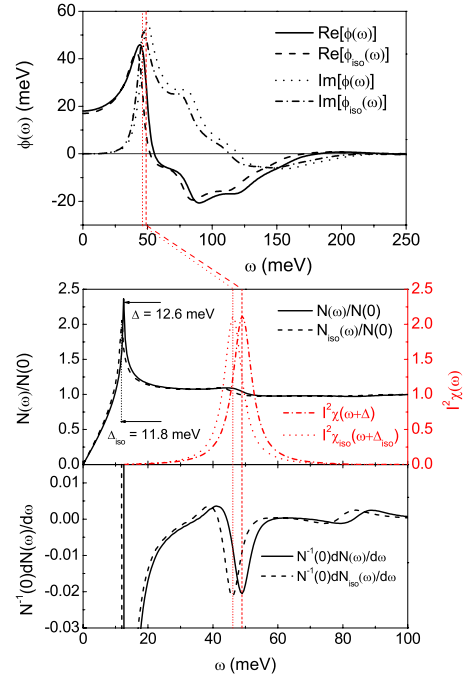


FIG. 2. (Color online) Top frame: the pairing energy $\phi(\omega)$ vs ω for an Eliashberg d -wave superconductor with the electron-boson interaction spectral density $\alpha^2F(\omega)$ [(red) dashed-dotted and dotted curves in the middle frame], a Lorentzian peaked at $\omega_L = 36.4$ meV displaced by the gap value $\Delta = 12.6$ meV at $T=10$ K with its isotope shifted value $\Delta_{\text{iso}} = 11.8$ meV. Middle frame: the quasiparticle density of states $N(\omega)/N(0)$ vs ω . Bottom frame: the first derivative $dN(\omega)/d\omega$ normalized to $N(0)$ vs ω .

the real part of the self-energy at the maximum is smaller for the ^{18}O case by $\sim 6\%$ reflecting the difference in A values. As ω increases the curves remain displaced as expected from our analysis of the Einstein spectrum case where the difference is related to a factor of γ^2 .

B. Superconducting state

The full nonlinear Eliashberg equations^{11,12,15,16} for a d -wave superconductor were solved for the gap and the renormalization function using the Lorentzian spectral function of Sec. II A as the nodal direction spectral density $\alpha^2F(\omega)$ and a temperature of $T=10$ K. The amplitude of the pairing energy $\phi(\omega)$ is energy dependent, and results for its real [(black) solid line] and imaginary part [(black) dotted line] are shown in the top frame of Fig. 2 where they are compared with the results for the isotopically substituted case [(black) dashed and dashed-dotted lines, respectively]. The peaks in both real and imaginary parts are around but not quite at $\omega_L + \Delta$. (See thin vertical lines which indicate the positions of $\omega_L + \Delta$ and $\omega_{L,\text{iso}} + \Delta_{\text{iso}}$ respectively.) Note also the small reduction in the value of the pairing energy at $\omega = 0$ for ^{18}O . The gaps Δ and Δ_{iso} which we identified as the position of the maximum in the quasiparticle density of states $N(\omega)/N(0)$ shown in the middle frame of Fig. 2 were equal to 12.6 and 11.8 meV, respectively, a 6% weakening. The critical temperature was $T_c = 54.5$ K and thus $2\Delta/(k_B T_c) = 5.35$ in our model calculations. Note the struc-

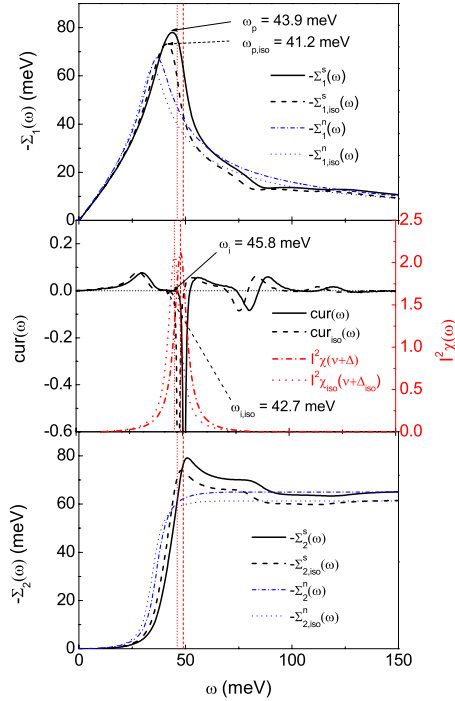


FIG. 3. (Color online) Top frame: minus the real part of the QP self-energy $-\Sigma_1^s(\omega)$ [(black) lines, left scale] for the superconducting state at temperature $T=10$ K vs ω . The calculations are based on a Lorentzian model for the electron-boson interaction spectral density $\alpha^2F(\omega)$ [see middle frame, (red) dashed-dotted and dotted lines, right-hand scale] displaced by the gap. The light (blue) dashed-dotted and dotted curves correspond to the normal-state results shown in the top frame of Fig. 1. Middle frame: curvature of $-\Sigma_1^s(\omega)$ vs ω . Bottom frame: the same as the top frame but for $-\Sigma_2^s(\omega)$.

ture in $N(\omega)/N(0)$ at the phonon energy shifted by the gap, i.e., with the peak in the electron-phonon spectral densities $\alpha^2F(\omega+\Delta)$ and $\alpha^2F_{iso}(\omega+\Delta_{iso})$, (red) dashed-dotted line and (red) dotted line, respectively. Furthermore, we find that the maxima match perfectly with the minima in the first derivative of the normalized quasiparticle density of states $N(0)^{-1}dN(\omega)/d\omega$ which is shown in the bottom frame of Fig. 2.

The superconducting state quasiparticle (QP) self-energy is shown in Fig. 3. In the top frame the (black) solid and dashed curves are the real part of the QP self-energy, $-\Sigma_1^s(\omega)$ and $-\Sigma_{1,iso}^s(\omega)$, respectively. For ease of comparison the thin (blue) dashed-dotted and dotted curves reproduce our normal state results of Fig. 1. The first important observation to be made is that the maxima in $-\Sigma_1^s(\omega)$ and $-\Sigma_{1,iso}^s(\omega)$ are at $\omega_p=43.9$ meV and $\omega_{p,iso}=41.2$ meV, respectively. These energies correspond *neither* to ω_L and $\omega_{L,iso}$ nor to $\omega_L+\Delta \sim 49$ meV and $\omega_{L,iso}+\Delta_{iso} \sim 46$ meV which are bigger. This illustrates the important fact that for a d -wave superconductor it is not easy to identify the position of a peak in $\alpha^2F(\omega)$ from the peak in the real part of the QP self-energy even if the gap value is known. While an isotropic gap can be identified, as we have done here from the peak in the QP density of states, the position of the peak in $-\Sigma_1^s(\omega)$ is not at $\omega_L+\Delta$ but rather in the particular case considered here falls

at a smaller energy; the shift is only 60% of Δ . Consequently, if the rule $\omega_L+\Delta$ is used on the position of the peak in the solid black curve in the top frame of Fig. 3 one would conclude that the peak in $\alpha^2F(\omega)$ is at 31.4 meV rather than at 36.4 meV.

The breakdown of the rule $\omega_L+\Delta$ to locate the maximum in the real part of the QP self-energy can be traced to a combination of the energy dependence of the QP density of states $N(\omega)$ (middle frame of Fig. 2) in a superconductor and our use of a distributed spectrum for $\alpha^2F(\omega)$ even though the model chosen for simplicity was a rather narrow Lorentzian form symmetric about ω_L .⁵³ For a pure δ -function spectral density there would indeed be a vertical drop in $-\Sigma_1^s(\omega)$ precisely at $\omega_L+\Delta$ as noted in the recent work by Lee *et al.*⁵⁴ The same vertical drop persists if a δ -function plus a smooth background is used as in the earlier work of Carbotte *et al.*¹⁶ but now the actual peak in $-\Sigma_1^s(\omega)$ is shifted to slightly lower energies. As we see in our Fig. 3 for a distributed spectrum the peak moved to even lower energy and a vertical drop at $\omega_L+\Delta$ is no longer identifiable. For broad spectra the relation between the position of the peak in $I^2F(\omega)$ and the peak in $-\Sigma_1^s(\omega)$ is even more complicated and depends on details beyond the values of ω_L and Δ , for example, on the asymmetry of the spectrum.⁵³ Finally, we note that, just as we saw in the normal state, the value of $-\Sigma_1^s(\omega)$ at maximum shifts downward by $\sim 6\%$ under $^{16}\text{O} \rightarrow ^{18}\text{O}$ substitution which reflects the shift in A value. At higher energies superconducting and normal curves meet but retain the γ^2 difference between ^{16}O and ^{18}O .

The bottom frame of Fig. 3 gives our results for $-\Sigma_2^s(\omega)$. The notation is the same as for the real part. A striking difference between normal and superconducting state is that now the main rise ends in a prominent maximum which reflects the maximum of the quasiparticle density of states in the superconductor. (See middle frame of Fig. 2.) In fact there is an easily identifiable image of $N(\omega)$ which is superimposed above the normal-state scattering rate. This image of $N(\omega)$ provides additional structure in $-\Sigma_2^s(\omega)$ not seen in the normal state. Reference to the thin vertical lines shows that the peak in $-\Sigma_2^s(\omega)$ does not align with the peak in $\alpha^2F(\omega+\Delta)$ as was also the case for the real part of the QP self-energy. The inflection points where the curvature of $-\Sigma_2^s(\omega)$ is zero falls at $\omega_i=45.8$ meV and $\omega_{i,iso}=42.7$ meV and are, therefore, not trivially correlated with the boson energy plus the gap value nor are they equal to the position of the maxima in the real part of the QP self-energy at ~ 44 and ~ 41 meV, respectively for ^{16}O and ^{18}O . These facts need to be kept in mind when analyzing experimental data.

Several features of the numerical simulations shown in Fig. 3 are incompatible with the recent ARPES data of Iwasawa *et al.*³⁵ Their data on the imaginary part of the quasiparticle self-energy shows no sign of saturating at energies above the maximum phonon energy in Bi2212 of ~ 86 meV, Ref. 55, but, instead, is increasing even at 200 meV and, most likely, beyond. Second, the data sets for ^{16}O and ^{18}O merge around 100 meV in contrast to our expectation for coupling predominantly to an oxygen phonon that they will remain displaced by $\sim 6\%$. A related observation can be made about the real part of the QP self-energy. The changes are mainly confined to the region 70–130 meV and,

in particular, the amplitude at maximum of the QP self-energy is found not to change significantly while we would expect a 6% change if we take our Lorentzian model as a representative for the sole coupling to a phonon mode.

While the analysis above rules out coupling to a single oxygen mode as the mechanism of superconductivity in the cuprates, such suggestions, nevertheless, keep appearing even in the most recent experimental literature. Examples include a model spectral density consisting predominantly of a single oxygen peak^{25,56} which has been considered in connection with the observation of a single mode at 52 meV showing a 6% shift on isotope substitution in the STM studies of Lee *et al.*²⁵ on the surface of Bi2212. Highly heterogeneous regions are found showing a variety of superconducting gap values. In each patch, structures are seen in the current-voltage characteristics (I - V characteristics) which are very similar to the phonon images of conventional superconductors. When the position in energy of these structures is carefully referenced to the gap energy, a dominant boson energy of $\Omega_B=52$ meV emerges. An alternate interpretation of these observations is that, what Lee *et al.*²⁵ observe is an inelastic tunneling process involving an oxygen phonon in the tunnel barrier layer.^{32–34} Such a phonon mode would have nothing to do with the glue causing the superconductivity in the CuO_2 layer and would remain silent on the isotope imprint data of Ref. 35. In a separate STM study²⁴ involving data collection above and below T_c , I - V characteristics could be normalized to the normal state. This procedure should cancel out matrix element effects and did produce density of state data which agrees well with that expected for a simple d -wave superconductor including inelastic damping. In all spectra deviations below the BCS prediction are seen and identified as boson structures. The average dip energy is found to be 35 meV for the Bi2212 sample studied. The magnitude of the boson structure observed as quantified by the magnitude of the deviation from BCS and was found not to scale with the size of the local superconducting gap in contrast to what is observed in conventional superconductors. Thus, it was concluded that they are not directly involved in the pairing glue. These experiments, however, remain silent as to the exact nature of these excitations.

III. OPTICAL SELF-ENERGY

For comparison with the quasiparticle case it is convenient to write the optical conductivity $\sigma(T, \omega)$ in terms of a complex optical self-energy $\Sigma^{op}(T, \omega) = \Sigma_1^{op}(T, \omega) + i\Sigma_2^{op}(T, \omega)$ via

$$\sigma(T, \omega) = i \frac{\Omega_p^2}{4\pi\omega} \frac{1}{-2\Sigma^{op}(T, \omega)} \quad (5)$$

with Ω_p the plasma frequency. The optical scattering rate $\tau_{op}^{-1}(T, \omega) = -2\Sigma_2^{op}(T, \omega)$ and the mass renormalization parameter $\lambda_{op}(T, \omega)$ is given by $\omega\lambda_{op}(T, \omega) = -2\Sigma_1^{op}(T, \omega)$. For zero temperature, coupling to a single Einstein mode at ω_L and the normal state as we have considered in Sec. II A we find

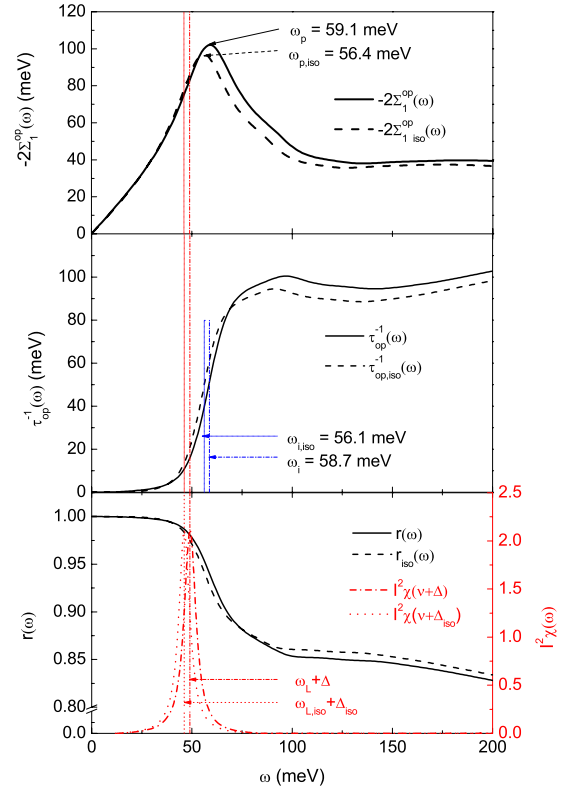


FIG. 4. (Color online) Top frame: minus twice the optical self-energy $-2\Sigma_1^{op}(\omega)$ vs energy ω in the superconducting state at $T=10$ K. The solid line corresponds to ^{16}O and the dashed one to ^{18}O . Middle frame: the same as the top frame but for the optical scattering rate $\tau_{op}^{-1}(\omega)$ vs energy ω . Bottom frame: the same as the top frame but for the reflectance $R(\omega)$ vs energy ω (left-hand scale applies). Dashed-dotted (red) (^{16}O) and (red) dotted (^{18}O) curves are the $\alpha^2 F(\omega)$ spectra displaced by the gap Δ and Δ_{iso} , respectively. The right-hand scale applies.

$$\tau_{op}^{-1}(T=0, \omega) = \frac{2\pi\gamma A}{\omega} (\omega - \gamma\omega_L) \theta(\omega - \gamma\omega_L) \quad (6)$$

and

$$-2\Sigma_1^{op}(T=0, \omega) = -2\gamma A \left[\ln \left| \frac{\omega + \gamma\omega_L}{\omega - \gamma\omega_L} \right| + \frac{\gamma\omega_L}{\omega} \ln \left| \frac{(\gamma\omega_L)^2 - \omega^2}{(\gamma\omega_L)^2} \right| \right], \quad (7)$$

where we have included the isotope factor γ . As in the quasiparticle case $\tau_{op}^{-1}(T=0, \omega)$ is zero up to $\omega = \gamma\omega_L$. At that point it starts out from zero but does not jump to its constant saturated value as for the quasiparticle case but rather rises toward $2\pi\gamma A$ only gradually as $(\omega - \gamma\omega_L)/\omega$. The onset of scattering is shifted down by 6% and its saturated value is also reduced by the same percentage. For the real part of the optical self-energy, $-2\Sigma_1^{op}(T=0, \omega)$, the slope into $\omega \rightarrow 0$ is unchanged by isotope substitution and is given by the same mass enhancement factor λ as in the quasiparticle case. The peak is positioned at $\sqrt{2}\gamma\omega_L$ and the amplitude at the peak position is reduced by 6%. Also isotope differences persist in

this quantity at large $\omega \gg \omega_L$ just as in Sec. II A. In Fig. 4 we show results for $-2\Sigma_1^{op}(T, \omega)$ (top frame) and $\tau_{op}^{-1}(T, \omega)$ (middle frame). The solid (black) line is for ^{16}O and the dashed for ^{18}O (left-hand scale). These curves are for the superconducting state at $T=10$ K and are based on the Lorentzian spectral density model of the previous section for the θ -averaged $I^2F(\omega)$ spectrum. As expected, the solid and dashed (black) curves for $-2\Sigma_1^{op}(T, \omega)$ merge as $\omega \rightarrow 0$. The peak frequency ω_p which is not at $\omega_L + \Delta$ shifts by 4.7% on oxygen isotope substitution and also drops in amplitude by 5%. Differences between the two curves, however, persist to the highest energy shown and are more significant than in the real part of the quasiparticle self-energy shown in the top frame of Fig. 3. As for $\tau_{op}^{-1}(T, \omega)$ (middle frame) it shows an onset which is shifted downward for ^{18}O . The solid and dashed (black) curves cross and then the ^{16}O and ^{18}O curves remain displaced in amplitude by 6%. Finally, the bottom frame presents our results for the reflectance $R(\omega)$

$$R(\omega) = \left| \frac{1 - \sqrt{\epsilon(\omega)}}{1 + \sqrt{\epsilon(\omega)}} \right|^2, \quad \epsilon(\omega) = \epsilon_\infty + i \frac{4\pi\sigma(\omega)}{\omega}, \quad (8)$$

where $\epsilon(\omega)$ is the dielectric function and ϵ_∞ is the dielectric constant at infinity. The results are for the plasma frequency $\Omega_p = 1$ eV and $\epsilon_\infty = 1$. The function $R(\omega)$ basically shows all features of an inverted optical scattering rate $\tau_{op}^{-1}(\omega)$, i.e., a sharp drop with onset around ~ 50 meV and saturation at the value of ~ 0.85 for energies > 100 meV. The isotope shift is well developed and should be observable by experiment. Such features are not seen in the optical data of Wang *et al.*³¹ in an underdoped $\text{YBa}_2\text{Cu}_3\text{O}_{7-\delta}$ sample. In particular, there is no evidence for a shift in frequency of the sharp drop in $R(\omega)$ around $400\text{--}500$ cm^{-1} . Thus, optics in this particular sample provides no evidence for a dominant oxygen-phonon contribution to $I^2F(\omega)$.

IV. APPLICATION TO Bi2212

We turn next to the explicit case of Bi2212 and base our discussion on the spectral density $I^2F(\omega)$ which we obtained previously from a maximum-entropy inversion¹¹ of the nodal direction ARPES data of Zhang *et al.*¹⁷ Results for the spectral density $I^2F(\omega)$ at temperature $T=17$ K in the superconducting state are reproduced in the bottom frame of Fig. 5 as the solid (black) line. Note first that this spectrum is very different from the single sharp Lorentzian form we have used so far. It has a broad peak around $\omega_L = 65$ meV but this is superimposed on a large background extending to 400 meV. In ARPES studies the cutoff in this spectrum depends critically on the choice of the bare dispersion curve since the renormalizations are taken to end at the crossing between bare and dressed dispersions and in the work of Zhang *et al.*¹⁷ this was 400 meV. This choice of cutoff is consistent with optical data.^{12–16} It is also consistent with the observation that the QP as well as optical scattering rates are still increasing with increasing ω even in the range of a few 100 meV. The maximum-entropy fit to the real part of the QP

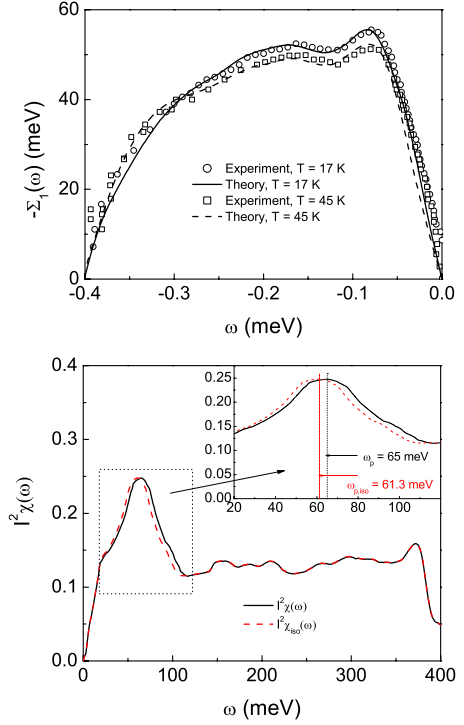


FIG. 5. (Color online) Top frame: fits to the real part of the superconducting state QP self-energy ARPES data of Zhou *et al.* (Ref. 17) as reported by Schachinger and Carbotte (Ref. 11). Bottom frame: the $I^2F(\omega)$ spectrum from maximum-entropy inversion of the $T=17$ K data (solid line) with $\lambda=1.19$, and the area under the spectrum $A=55.1$ meV. The (red) dashed line shows the spectrum $I^2F_{\text{iso}}(\omega)$ which was used to simulate the isotope effect. As indicated in the inset only the entire peak area is shifted in energy by 6% with $\lambda=1.19$ and $A_{\text{iso}}=54.8$ meV. The area under the shifted peak is 6.15 meV which corresponds to a $\lambda=0.21$.

self-energy is shown in the top frame of Fig. 5 for two temperatures, namely, $T=17$ and 45 K. The data are indicated by open circles and open squares, respectively. The overall fit is excellent. No attempt was made to get the closest possible fit to the peak position but this is of no importance for what follows. The finite band nature of the electronic structure was taken into account with a band width of 1.2 eV. To simulate the effect of an isotope substitution we shifted the entire area of the peak by 6% in energy to $\omega_{L,\text{iso}}=61.3$ meV making sure that the resulting mass enhancement λ is left unchanged [the area under the curves, solid (black) and dashed (red) in the inset of the bottom frame of Fig. 6 is reduced by 6% though]. This results in a shift of the gap from $\Delta = 26.1$ meV to $\Delta_{\text{iso}} = 25.8$ meV which is almost negligible. The resulting value of the real part of the QP self-energy, dashed (red) curve, in the nodal direction is compared with its unshifted [solid (black)] curve in the top frame of Fig. 6. We see that the peak shifts by about 5% as we expected and also that the dashed curve falls below the solid curve in the region of the peak. The results are in good agreement with the experimental data of Iwasawa *et al.*³⁵ for the shift in peak position but the amplitude of the peak is reduced more than in the experiments and we will return to this issue below. Thus, we can conclude that it is sufficient to shift a small part

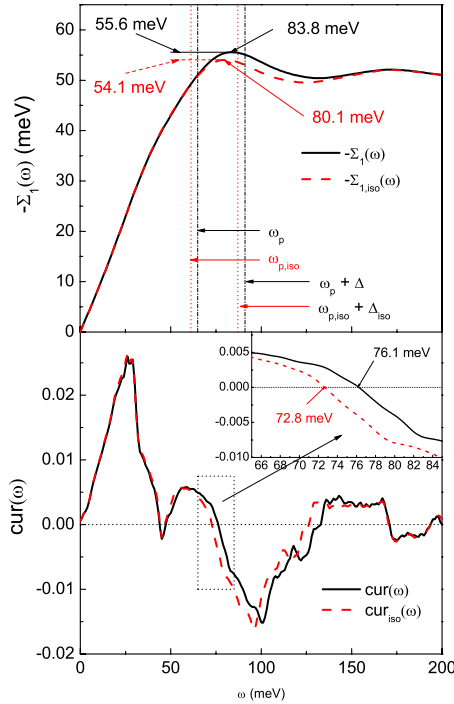


FIG. 6. (Color online) Top frame: the real part of the optical self-energy $-\Sigma_1(\omega)$ vs ω of Bi2212 in the superconducting state at $T=17$ K. The (black) solid line is based on the $I^2F(\omega)$ spectrum shown in the bottom frame of Fig. 5 and the (red) dashed line corresponds to $I^2F_{iso}(\omega)$. The peak position shifts down by $\sim 5\%$ and the amplitude at the peak position by $<3\%$. Bottom frame: the same as the top frame but for the curvature $\text{cur}(\omega)$ of the imaginary part of the self-energy highlighting in the inset the shift of $\sim 4\%$ in the inflection point due to the isotope effect.

of the $I^2F(\omega)$ in order to understand these experimental results. In the bottom frame of Fig. 6 we show results for the corresponding imaginary part of the quasiparticle self-energy. What is presented is the curvature of $-\Sigma_2(\omega)$ from which we can identify a shift in the energy of its zero value, the inflection point, from 76.1 to 72.8 meV. This gives an independent measure of the isotope shift in the quasiparticle properties. It is important to emphasize, again, that the peak in the real part and the inflection point of the imaginary part of the self-energy are not quite at the same energies and are not trivially correlated with each other.

The area under the electron-boson spectral density which we have shifted in energy by 6% and which is shown in the inset of the bottom frame of Fig. 5 corresponds to 6.13 meV or about 10% of the total area under the $I^2F(\omega)$ that we have used to describe the electron-boson coupling in the nodal direction of Bi2212. If we associated this shift in area entirely to an electron-phonon coupling, the mass enhancement factor involved is $\lambda \approx 0.2$. This value is much smaller than estimated in Ref. 35 but is of the order found in band-structure calculations on related cuprates.^{57–61} It also compares favorably with the total value of mass enhancement $\lambda_{tot}=0.23$ found in studies⁶² of anisotropic electron-phonon coupling due to the oxygen buckling mode (~ 36 meV). The coupling to the breathing mode (~ 70 meV) was found to be

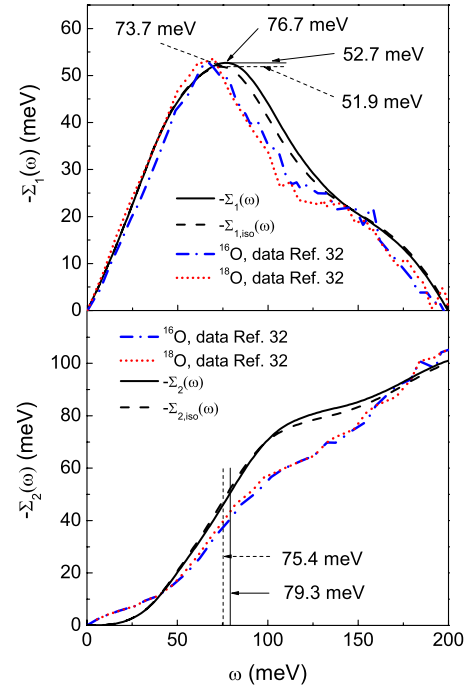


FIG. 7. (Color online) Top frame: the real part of the QP self-energy $-\Sigma_1(\omega)$ vs ω of Bi2212 in the superconducting state at $T=17$ K for a $I^2F(\omega)$ spectrum cut off at 200 meV (solid line). The (black) dashed line is the corresponding ^{18}O result. The peak position shifts by $\sim 4\%$ and the amplitude at the peak position drops by less than one meV. The (blue) dashed-dotted line presents the ^{16}O ARPES data of Iwasawa *et al.* (Ref. 35) and the (red) dotted line is the ^{18}O ARPES data. Bottom frame: the same as the top frame but for the imaginary part of the QP self-energy $-\Sigma_2(\omega)$. The inflection points are indicated by the two thin solid and dashed vertical lines.

much smaller: $\lambda_{tot} \sim 0.02$. Our value of $\lambda=0.2$ corresponds to less than 20% of the total λ found through maximum entropy inversion¹¹ of the nodal direction ARPES data of Ref. 17.

In a last step we investigate how an energy cutoff of 200 meV on the QP self-energy which was used by Iwasawa *et al.*³⁵ influences data analysis and interpretation. For this purpose we performed a numerical simulation based on the $I^2F(\omega)$ spectrum presented by the solid line in the bottom frame of Fig. 5 but which has been cut off at 200 meV. (Such a cutoff is the logical consequence of the 200 meV energy cutoff applied on the real part of the QP self-energy when such data are inverted.) In this simulation we will make an attempt to reproduce as closely as possible the effect the isotope substitution has on the imaginary part of the self-energy as discussed by Iwasawa *et al.*³⁵ It is based on the solution of finite band d -wave Eliashberg equations as they have been discussed by Schachinger and Carbotte.¹¹ This task requires consideration of three parameters, namely, the mass enhancement parameter λ , the parameter g which accounts for the fact that the projection of the electron-boson spectral density will, in general, be different for the renormalized frequencies and the renormalized pairing potential. The third parameter to be adjusted is the band width W . Constraints are the correct value of the critical temperature $T_c=92$ K and a best possible reproduction of the experimental $-\Sigma_2(\omega)$ ^{16}O ARPES data. Figure 7 presents the results of

this simulation. The best agreement with experiment was achieved for $\lambda=1.33$, $g=1.22$ (so far, for simplicity, g was set to one throughout the paper), and $W=0.6$ eV a substantial reduction from the previous value of 1.2 eV. Due to the cutoff of 200 meV the area A under the $I^2F(\omega)$ spectrum is reduced from 55.1 to 38 meV and $A_{\text{iso}}=37.6$ meV, down from 54.8 meV. The area under the shifted peak increased to 8.11 meV which corresponds to a $\lambda=0.26$. Thus, the area under the shifted peak is now about 20% of the total area while it was only about 10% in the bottom frame of Fig. 5 with the energy cutoff at 400 meV. Finally, the gap amplitude $\Delta=33.1$ meV and $\Delta_{\text{iso}}=32.7$ meV up by about 7 meV which we can trace to the increased value of g .

The top frame of Fig. 7 presents our results for the real part of the QP self-energy. The solid (black) curve is for ^{16}O and is equivalent to the solid (black) line in the top frame of Fig. 6 except that now an energy cutoff of 200 meV was used. The dashed (black) line is for the ^{18}O isotope. The (blue) dashed-dotted curve shows the ^{16}O ARPES data and was read off Fig. 2(b) of Iwasawa *et al.*³⁵ It corresponds to their cut zero which is exactly in the nodal direction. As the data are given only in arbitrary units we rescaled them to match the maximum of our solid (black) curve, i.e., 52.7 meV. The dotted (red) curve shows the ^{18}O ARPES data and was rescaled by the same factor as the ^{16}O data. The result of our simulation is that the peak in the real part of the self-energy which corresponds to the (unchanged) peak $\omega_L=65$ meV in the $I^2F(\omega)$ moves down from 83.8 to 76.7 meV as a result of the reduced energy cutoff, despite the fact that the gap amplitude has increased by ~ 7 meV. The isotope effect still accounts for a further shift of this peak by about 3 down to 73.7 meV. This remains in good agreement with the experimental shift of 3.4 ± 0.5 meV quoted by Iwasawa *et al.*³⁵

It is also important to notice the over all good qualitative agreement of the numerical simulation with the ARPES data. In particular, the weak depression at ~ 120 meV which is followed by a soft bump extending to ~ 200 meV is clearly seen at about the same energies in the ARPES data. This weak structure is the 200 meV cutoff equivalent of the pronounced peak-valley-hump structure seen in the top frame of Fig. 5. Furthermore, we see that the amplitudes of the real part of the QP self-energy at the peak positions now differ by less than 1 meV which is below the ARPES accuracy and, thus, cannot be picked up by experiment. In the case of the 400 meV cutoff this difference was about 1.5 meV.

The bottom frame of Fig. 7 shows the result of our simulation for the imaginary part of the self-energy. The solid (black) line corresponds to ^{16}O and the dashed (black) line to ^{18}O . We included for comparison ARPES data reported by Iwasawa *et al.*³⁵ read off their Fig. 3(b). The dashed-dotted (blue) line is for ^{16}O and the dotted (red) line is for ^{18}O . The qualitative agreement is quite good and it is remarkable that the inflection point in our simulated results moved up to 79.3 and 75.4 meV, respectively, in comparison to our result of the 400 meV cutoff results shown in the bottom frame of Fig. 6. Iwasawa *et al.*³⁵ quote the isotope effect of the inflection point as 3.2 ± 0.6 meV and our simulation is in reasonable agreement with their observation albeit the energy of our inflection point is well above the position quoted by Iwasawa

et al. Most importantly, the ARPES data as well as the simulation indicate that $-\Sigma_2(\omega)$ keeps increasing beyond 200 meV. This is a very clear indication that the $I^2F(\omega)$ spectrum extends to high energies. If it were restricted to the maximum phonon energy of ~ 85 meV, Ref. 55, we should experience a saturation of $-\Sigma_2(\omega)$ already at energies well below 200 meV. Nevertheless, we would like to point out that there is a pronounced disagreement between theoretical predictions and experimental data for $-\Sigma_2(\omega)$ in the energy interval $50 \leq \omega \leq 170$ meV while we achieve much better agreement in the same interval for $-\Sigma_1(\omega)$. This could be related to the fact that the experimental data for $-\Sigma_1(\omega)$ and $-\Sigma_2(\omega)$ are not quite Kramers-Kronig related while theory is.

This numerical simulation demonstrates that moving the energy cutoff down from 400 to 200 meV has quite a serious effect on data analysis. Most importantly the peak position in the real part of the self-energy is moved toward lower energies thus indicating a different position ω_L of the corresponding peak in the $I^2F(\omega)$ spectrum as compared with data generated using a 400 meV cutoff. This observation is even valid when the strict rule that the kink appears at the mode energy ω_L plus the gap amplitude Δ is applied.

Finally, the good qualitative agreement of the numerical simulation with the ARPES data by Iwasawa *et al.*³⁵ allows us to conclude that the $I^2F(\omega)$ spectrum which underlies this data will be quite similar to what we found from inversion of the ARPES data by Zhang *et al.*¹⁷ shown in the bottom frame of Fig. 5. The peak position ω_L can be estimated quite safely from our simulation to be somewhere between 55 and 58 meV. This energy is not in agreement with the two possible candidates for the isotope effect, the oxygen buckling mode with ~ 36 meV and the oxygen breathing mode with ~ 69 meV. We turn next to optics.

The normal state optical self-energy $\Sigma_1^{op}(\omega)$ of an optimally doped Bi2212 sample was inverted by van Heumen *et al.*⁶³ to find the electron-boson spectral function $I^2F(\omega)$. They report a pronounced peak centered around ~ 60 meV well separated from a broad background which extends up to 400 meV. The peak position and its amplitude barely change with temperature in the regime $100 \leq T \leq 300$ K. This resulted in the obvious interpretation that this peak in the $I^2F(\omega)$ spectrum is due to the interaction of the charge carriers with a phonon. Nevertheless, they conclude that the contribution of the electron-phonon coupling to the pairing is too small to account for the observed critical temperature and that the part of the $I^2F(\omega)$ spectrum at energies above 100 meV is of crucial importance for the pairing mechanism. In contrast to this study, Hwang *et al.*¹³ inverted the optical scattering rate of an optimally doped Bi2212 sample using a maximum-entropy technique.¹² They also found a pronounced peak centered around ~ 60 meV at low temperatures but its amplitude decreases and its position moves to higher energies with increasing temperatures. At $T=300$ K the peak becomes almost completely smeared out. Such a result is more in line with the interpretation that the peak in $I^2F(\omega)$ is caused by the coupling of the charge carriers to a spin-one resonance. As the inversion process by itself is an ill-posed problem both solutions are valid and studying the optical properties of an isotope substituted Bi2212 sample may provide the required independent information which

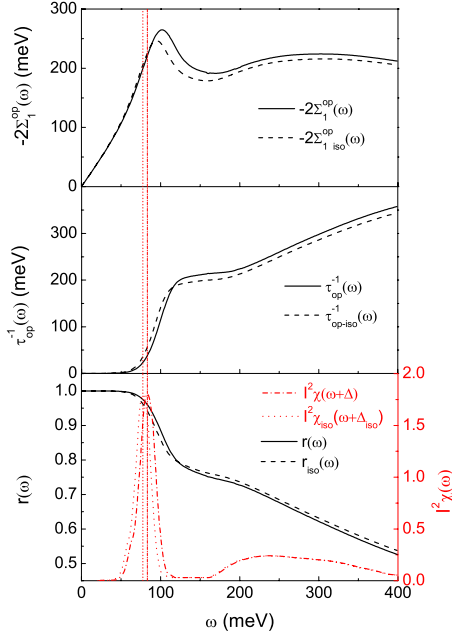


FIG. 8. (Color online) Top frame: minus twice the optical self-energy $-2\Sigma_1^{op}(\omega)$ vs energy ω for an optimally doped Bi2212 sample in the superconducting state at $T=27$ K. The solid line corresponds to ^{16}O and the dashed one to ^{18}O . Middle frame: the same as the top frame but for the optical scattering rate $\tau_{op}^{-1}(\omega)$ vs energy ω . Bottom frame: the same as the top frame but for the reflectance $R(\omega)$ vs energy ω (left-hand scale applies). (Red) dashed-dotted (^{16}O) and (red) dotted (^{18}O) lines are the $I^2F(\omega)$ spectra displaced by the gap $\Delta=22.7$ meV and $\Delta_{iso}=20.66$ meV, respectively. The left-hand scale applies.

will in the end allow one to discriminate between these two scenarios.

We propose here that it should be sufficient to study the optical properties of such an isotope-substituted Bi2212 sample in the superconducting state. To demonstrate this, the main peak in the $I^2F(\omega)$ spectrum reported by Hwang *et al.*¹³ for $T=27$ K has been shifted down in energy by 6% to simulate the effect of the $^{16}\text{O} \rightarrow ^{18}\text{O}$ isotope substitution. The rest of the spectrum at energies >110 meV stayed unchanged. The two spectra are shown in the bottom frame of Fig. 8 with the (red) dashed-dotted line presenting the ^{16}O spectrum and the (red) dotted line for the ^{18}O spectrum. (The right-hand scale applies.) Note that the spectra have been shifted in energy by $\Delta=22.7$ meV and $\Delta_{iso}=20.7$ meV, respectively. The most significant changes are observed in the results for the real part of the optical self-energy $-2\Sigma_1^{op}(\omega)$ presented in the top frame of Fig. 8 (solid line for ^{16}O and dashed line for ^{18}O). The result is very similar to what has already been discussed in the top frame of Fig. 4 for the cut-off Lorentzian spectrum. Now there is a very pronounced peak in $-2\Sigma_1^{op}(\omega)$ at $\omega \sim 100$ meV which gets shifted down to ~ 94 meV and we also see quite a reduction in the peak amplitude from 264.8 to 246.3 meV due to isotope substitution. These signals are strong enough to be seen in optical experiments and the existence/nonexistence of this signal will then allow one to discriminate between the two possible scenarios discussed by van Heumen *et al.*⁶³ and Hwang *et al.*¹³ The changes in

the optical scattering rate shown in the middle frame of Fig. 8 and in the reflectivity shown in the bottom frame of the same figure are also large and measurable.

One should, finally, keep in mind the possibility that some of the sensitivity to isotope substitution seen in Ref. 35 could be due to a modulation of the exchange interaction J by the zero-point vibrations of the oxygen ions. This possibility was considered by Plakida.⁶⁴ The Néel temperature in undoped La_2CuO_4 is known to change on ^{18}O substitution for ^{16}O , Ref. 65, and this implies that the exchange constant J will be changed and, consequently, so will the spin fluctuations which themselves depend on J . But details of this relationship have not yet been worked out. In this context, recent calculations based on the Hubbard and t - J models^{42,43} find spin-fluctuation spectra which are very similar to the ones obtained from inversion of quasiparticle and optical data which we have used here for Bi2212. On the other hand, a neutron study of the 41 meV spin-one resonance in $\text{YBa}_2\text{Cu}_3\text{O}_{6.89}$ by Pailhès *et al.*⁶⁶ found no shift on isotope substitution in agreement with the result reported by Wang *et al.*³¹

V. CONCLUSION

We analyzed very recent nodal direction ARPES data of the effect of $^{16}\text{O} \rightarrow ^{18}\text{O}$ substitutions on the quasiparticle self-energy. An Eliashberg formalism is employed to relate renormalizations to an effective charge-carrier boson interaction spectral function $I^2F(\omega)$. For the superconducting state it is assumed that the gap has d -wave symmetry. Through numerical simulations we find that the data is inconsistent with a model for $I^2F(\omega)$ which consists dominantly of coupling to a single oxygen mode. A more realistic model is based on a previous maximum-entropy inversion of nodal direction self-energy ARPES data of Zhang *et al.*¹⁷ in the energy range up to 400 meV. The electron-boson spectral density consists in this case of a broad peak around 65 meV superimposed on a large, mainly structureless background extending to 400 meV, the cutoff in the data. When only the area under the peak which accounts for about 10% of the total is assigned to phonons and is shifted, leaving the remainder unchanged, we obtain reasonable agreement with the oxygen-substituted ARPES data. If the mass enhancement parameter λ is used instead of the area under $I^2F(\omega)$ as a measure of the strength of the electronic renormalizations, the phonon contribution to λ is 0.2 or less than 20% of the total $\lambda=1.19$ based on a realistic model for the spectral density in Bi2212 obtained from inversion of nodal direction ARPES quasiparticle self-energy data. We conclude that the new measurements of Ref. 35 do not imply that the phonons play a large role in the superconductivity of this class of materials. In our model 90% of the area under $I^2F(\omega)$ is assigned to a spin fluctuation background.

We also provided an equivalent analysis based on optical data. The relevant momentum-averaged electron-boson spectral density was taken from optical scattering-rate data and shows a pronounced peak around 60 meV in Bi2212. We argue that if this peak is entirely assigned to coupling to an oxygen phonon as some authors would imply⁵⁶ large, easily

measurable changes would result in the reflectivity as a function of energy as well as in the corresponding optical self-energy. To our knowledge this has not yet been observed. Experimental data³¹ does exist in the related case of underdoped $\text{YBa}_2\text{Cu}_3\text{O}_{6+\delta}$ where no effect of $^{16}\text{O} \rightarrow ^{18}\text{O}$ substitution is observed within the precision of the experiment.

ACKNOWLEDGMENTS

Research supported in part by the Natural Sciences and Engineering Research Council of Canada (NSERC) and by the Canadian Institute for Advanced Research (CIFAR). We want to thank T. Timusk for interest and discussions.

*schachinger@itp.tu-graz.ac.at

- ¹T. Cuk, F. Baumberger, D. H. Lu, N. Ingle, X. J. Zhou, H. Eisaki, N. Kaneko, Z. Hussain, T. P. Devereaux, N. Nagaosa, and Z.-X. Shen, *Phys. Rev. Lett.* **93**, 117003 (2004).
- ²X. J. Zhou, J. Shi, T. Yoshida, T. Cuk, W. L. Yang, V. Brouet, J. Nakamura, N. Mannella, S. Komiya, Y. Ando, F. Zhou, W. X. Ti, J. W. Xiong, Z. X. Zhao, T. Sasagawa, T. Kakeshita, H. Eisaki, S. Uchida, A. Fujimori, Z. Zhang, E. W. Plummer, R. B. Laughlin, Z. Hussain, and Z.-X. Shen, *Phys. Rev. Lett.* **95**, 117001 (2005).
- ³W. Meevasana, N. J. C. Ingle, D. H. Lu, J. R. Shi, F. Baumberger, K. M. Shen, W. S. Lee, T. Cuk, H. Eisaki, T. P. Devereaux, N. Nagaosa, J. Zaanen, and Z.-X. Shen, *Phys. Rev. Lett.* **96**, 157003 (2006).
- ⁴P. D. Johnson, T. Valla, A. V. Fedorov, Z. Yusof, B. O. Wells, Q. Li, A. R. Moodenbaugh, G. D. Gu, N. Koshizuka, C. Kendziora, S. Jian, and D. G. Hinks, *Phys. Rev. Lett.* **87**, 177007 (2001).
- ⁵T. Valla, T. E. Kidd, W.-G. Yin, G. D. Gu, P. D. Johnson, Z.-H. Pan, and A. V. Fedorov, *Phys. Rev. Lett.* **98**, 167003 (2007).
- ⁶S. R. Park, D. J. Song, C. S. Leem, C. Kim, C. Kim, B. J. Kim, and H. Eisaki, *Phys. Rev. Lett.* **101**, 117006 (2008).
- ⁷A. D. Gromko, A. V. Fedorov, Y.-D. Chuang, J. D. Koralek, Y. Aiura, Y. Yamaguchi, K. Oka, Y. Ando, and D. S. Dessau, *Phys. Rev. B* **68**, 174520 (2003).
- ⁸T. Sato, H. Matsui, T. Takahashi, H. Ding, H.-B. Yang, S.-C. Wang, T. Fujii, T. Watanabe, A. Matsuda, T. Terashima, and K. Kadowaki, *Phys. Rev. Lett.* **91**, 157003 (2003).
- ⁹S. V. Borisenko, A. A. Kordyuk, T. K. Kim, A. Koitzsch, M. Knupfer, M. S. Golden, J. Fink, M. Eschrig, H. Berger, and R. Follath, *Phys. Rev. Lett.* **90**, 207001 (2003).
- ¹⁰A. A. Kordyuk, S. V. Borisenko, V. B. Zabolotnyy, J. Geck, M. Knupfer, J. Fink, B. Buchner, C. T. Lin, B. Keimer, H. Berger, A. V. Pan, S. Komiya, and Y. Ando, *Phys. Rev. Lett.* **97**, 017002 (2006).
- ¹¹E. Schachinger and J. P. Carbotte, *Phys. Rev. B* **77**, 094524 (2008).
- ¹²E. Schachinger, D. Neuber, and J. P. Carbotte, *Phys. Rev. B* **73**, 184507 (2006).
- ¹³J. Hwang, T. Timusk, E. Schachinger, and J. P. Carbotte, *Phys. Rev. B* **75**, 144508 (2007).
- ¹⁴J. Hwang, E. Schachinger, J. P. Carbotte, F. Gao, D. B. Tanner, and T. Timusk, *Phys. Rev. Lett.* **100**, 137005 (2008).
- ¹⁵E. Schachinger, C. C. Homes, R. P. S. M. Lobo, and J. P. Carbotte, *Phys. Rev. B* **78**, 134522 (2008).
- ¹⁶J. P. Carbotte, E. Schachinger, and J. Hwang, *Phys. Rev. B* **71**, 054506 (2005).
- ¹⁷W. Zhang, G. Liu, L. Zhao, H. Liu, J. Meng, X. Dong, W. Lu, J. S. Wen, Z. J. Xu, G. D. Gu, T. Sasagawa, G. Wang, Y. Zhu, H. Zhang, Y. Zhou, X. Wang, Z. Zhao, C. Chen, Z. Xu, and X. J. Zhou, *Phys. Rev. Lett.* **100**, 107002 (2008).
- ¹⁸E. Schachinger and J. P. Carbotte, *Phys. Rev. B* **62**, 9054 (2000).
- ¹⁹E. Schachinger, J. J. Tu, and J. P. Carbotte, *Phys. Rev. B* **67**, 214508 (2003).
- ²⁰E. Schachinger, J. P. Carbotte, and T. Timusk, *EPL* **86**, 67003 (2009).
- ²¹J. F. Zasadzinski, L. Ozyuzer, N. Miyakawa, K. E. Gray, D. G. Hinks, and C. Kendziora, *Phys. Rev. Lett.* **87**, 067005 (2001).
- ²²J. F. Zasadzinski, L. Ozyuzer, L. Coffey, K. E. Gray, D. G. Hinks, and C. Kendziora, *Phys. Rev. Lett.* **96**, 017004 (2006).
- ²³F. C. Niestemski, S. Kunwar, S. Zhou, S. Li, H. Ding, Z. Wang, P. Dai, and V. Madhavan, *Nature (London)* **450**, 1058 (2007).
- ²⁴A. N. Pasupathy, A. Pushp, K. K. Gomes, C. V. Parker, J. Wen, Z. Xu, G. Gu, S. Ono, Y. Ando, and A. Yazdani, *Science* **320**, 196 (2008).
- ²⁵J. Lee, K. Fujita, K. McElroy, J. A. Slezak, M. Wang, Y. Aiura, H. Bando, M. Ishikado, T. Masui, J. X. Zhu, A. V. Balatsky, H. Eisaki, S. Uchida, and J. C. Davis, *Nature (London)* **442**, 546 (2006).
- ²⁶J. P. Franck, in *Physical Properties of High Temperature Superconductors III*, edited by D. M. Ginsberg (World Scientific, Singapore, 1994), p. 189.
- ²⁷E. Schachinger, M. G. Greeson, and J. P. Carbotte, *Phys. Rev. B* **42**, 406 (1990).
- ²⁸T. Dahm, *Phys. Rev. B* **61**, 6381 (2000).
- ²⁹A. Lanzara, P. V. Bogdanov, X. J. Zhou, S. A. Kellar, D. L. Feng, E. D. Lu, T. Yoshida, H. Eisaki, A. Fujimori, K. Kishio, J. I. Shimoyama, T. Noda, S. Uchida, Z. Hussain, and Z. X. Shen, *Nature (London)* **412**, 510 (2001).
- ³⁰G. H. Gweon, T. Sasagawa, S. Y. Zhou, J. Graf, H. Takagi, D. H. Lee, and A. Lanzara, *Nature (London)* **430**, 187 (2004).
- ³¹N. L. Wang, T. Timusk, J. P. Franck, P. Schweiss, M. Braden, and A. Erb, *Phys. Rev. Lett.* **89**, 087003 (2002).
- ³²D. J. Scalapino, *Nat. Phys.* **2**, 593 (2006).
- ³³J. Hwang, T. Timusk, and J. P. Carbotte, *Nature (London)* **446**, E3 (2007).
- ³⁴S. Pilgram, T. M. Rice, and M. Sigrist, *Phys. Rev. Lett.* **97**, 117003 (2006).
- ³⁵H. Iwasawa, J. F. Douglas, K. Sato, T. Masui, Y. Yoshida, Z. Sun, H. Eisaki, H. Bando, A. Ino, M. Arita, K. Shimada, H. Namatame, M. Taniguchi, S. Tajima, S. Uchida, T. Saitoh, D. S. Dessau, and Y. Aiura, *Phys. Rev. Lett.* **101**, 157005 (2008).
- ³⁶J. P. Carbotte, *Rev. Mod. Phys.* **62**, 1027 (1990).
- ³⁷E. J. Nicol, J. P. Carbotte, and T. Timusk, *Phys. Rev. B* **43**, 473 (1991).
- ³⁸J. P. Carbotte, C. Jiang, D. N. Basov, and T. Timusk, *Phys. Rev. B* **51**, 11798 (1995).
- ³⁹F. Marsiglio, J. P. Carbotte, A. Puchkov, and T. Timusk, *Phys. Rev. B* **53**, 9433 (1996).

- ⁴⁰E. Schachinger, J. P. Carbotte, and F. Marsiglio, Phys. Rev. B **56**, 2738 (1997).
- ⁴¹A. V. Chubukov, D. Pines, and J. Schmalian, in *Superconductivity, Conventional and Unconventional Superconductors*, edited by K. H. Bennemann and J. B. Ketterson (Springer, New York, 2004), Vol. 2, Chap. 22, p. 1349.
- ⁴²T. A. Maier, D. Poilblanc, and D. J. Scalapino, Phys. Rev. Lett. **100**, 237001 (2008).
- ⁴³B. Kyung, D. Sénéchal, and A.-M. S. Tremblay, Phys. Rev. B **80**, 205109 (2009).
- ⁴⁴P. W. Anderson, Science **316**, 1705 (2007).
- ⁴⁵J. P. Carbotte and E. Schachinger, J. Low Temp. Phys. **144**, 61 (2006).
- ⁴⁶E. Schachinger and J. P. Carbotte, Phys. Rev. B **72**, 014535 (2005).
- ⁴⁷E. J. Nicol and J. P. Carbotte, Phys. Rev. B **44**, 7741(R) (1991).
- ⁴⁸B. Mitrović and J. P. Carbotte, Can. J. Phys. **61**, 758 (1983).
- ⁴⁹B. Mitrović and J. P. Carbotte, Can. J. Phys. **61**, 789 (1983).
- ⁵⁰A. Knigavko and J. P. Carbotte, Phys. Rev. B **72**, 035125 (2005).
- ⁵¹A. Knigavko and J. P. Carbotte, Phys. Rev. B **73**, 125114 (2006).
- ⁵²B. Mitrović and J. P. Carbotte, Solid State Commun. **40**, 249 (1981).
- ⁵³E. Schachinger and J. P. Carbotte, Phys. Rev. B **80**, 094521 (2009).
- ⁵⁴W. S. Lee, W. Meevasana, S. Johnston, D. H. Lu, I. M. Vishik, R. G. Moore, H. Eisaki, N. Kaneko, T. P. Devereaux, and Z. X. Shen, Phys. Rev. B **77**, 140504(R) (2008).
- ⁵⁵B. Renker, F. Gompf, D. Ewert, P. Adelman, H. Schmidt, E. Gering, and H. Mutka, Z. Phys. B: Condens. Matter **77**, 65 (1989).
- ⁵⁶A. de Lozanne, Nature (London) **442**, 522 (2006).
- ⁵⁷S. Y. Savrasov and O. K. Andersen, Phys. Rev. Lett. **77**, 4430 (1996).
- ⁵⁸K. P. Bohnen, R. Heid, and M. Krauss, Europhys. Lett. **64**, 104 (2003).
- ⁵⁹R. Heid, K.-P. Bohnen, R. Zeyher, and D. Manske, Phys. Rev. Lett. **100**, 137001 (2008).
- ⁶⁰F. Giustino, M. L. Cohen, and S. G. Louie, Nature (London) **452**, 975 (2008).
- ⁶¹R. Heid, R. Zeyher, D. Manske, and K.-P. Bohnen, Phys. Rev. B **80**, 024507 (2009).
- ⁶²T. P. Devereaux, T. Cuk, Z.-X. Shen, and N. Nagaosa, Phys. Rev. Lett. **93**, 117004 (2004).
- ⁶³E. van Heumen, E. Muhlethaler, A. B. Kuzmenko, H. Eisaki, W. Meevasana, M. Greven, and D. van der Marel, Phys. Rev. B **79**, 184512 (2009).
- ⁶⁴N. M. Plakida, JETP Lett. **74**, 36 (2001).
- ⁶⁵G.-m. Zhao, K. K. Singh, and D. E. Morris, Phys. Rev. B **50**, 4112 (1994).
- ⁶⁶S. Pailhès, P. Bourges, Y. Sidis, C. Bernhard, B. Keimer, C. T. Lin, and J. L. Tallon, Phys. Rev. B **71**, 220507(R) (2005).